Structure of the Reduced $TiO_2(110)$ Surface Determined by Scanning Tunneling Microscopy

GREGORY S. ROHRER,* VICTOR E. HENRICH, DAWN A. BONNELL

The scanning tunneling microscope has been used to image a reduced $TiO_2(110)$ surface in ultrahigh vacuum. Structural units with periodicities ranging from 21 to 3.4 angstroms have been clearly imaged, demonstrating that atomic resolution imaging of an ionic, wide band gap (3.2 electron volts) semiconductor is possible. The observed surface structures can be explained by a model involving ordered arrangements of two-dimensional defects known as crystallographic shear planes and indicate that the topography of nonstoichiometric oxide surfaces can be complex.

TRANSITION METAL OXIDE SURFACES play an important role in a number of phenomena, including heterogeneous catalysis, gas sensing, electrode-electrolyte interactions, and bonding at metal-ceramic interfaces. However, in comparison to the current knowledge of metallic and covalently bonded semiconductor surfaces, little is known about transition metal oxide surfaces. Notable successes among the few scanning tunneling microscope (STM) studies of oxides include the atomic or near-atomic resolution imaging of four different metallic oxide surfaces (*1*) and the imaging of some atomic-scale features on the surface of $Rb_{0.05}WO_3$, a semiconducting tungsten bronze (*2*).

We have used the STM to study the geometric and electronic structure of the $TiO_2(110)$ surface, a wide band gap, semiconducting oxide. We acquired images from a single-crystal $TiO_2(110)$ sample that was cleaned and annealed in ultrahigh vacuum (UHV), conditions necessary to avoid the adsorption, band bending, and charging effects that are known to occur in air. Several well-ordered areas have been imaged that contain a variety of atomic-scale, periodic structures. Although none of these features correlates with the expected surface structure, all are consistent with a model involving the presence of crystallographic shear (CS) planes that accommodate local variations in stoichiometry. We briefly describe two of the observed structures and compare them to the proposed model.

Titania can support a wide range of oxygen deficiency (TiO_{2-x}, $x = 0$ to 0.33) through the formation of planar defects known as CS planes, which, when numerous enough, order to form new compounds with distinct compositions and structures that are known as Magneli phases (*3*). The general formula for these compounds, which can occur as intergrowths in reduced crystals, is Ti_nO_{2n-1} where $n \geq 3$. The *n*th-order CS structure may be formed by creating O vacancies at the anion sites in every 2*n*th shear plane [for example, the $(1\bar{2}1)$ plane] and displacing the adjacent rutile section by $\frac{1}{2}[0\bar{1}1]$. The result is that the approximately close-packed O framework remains continuous but the Ti cations are in antiphase locations, with increased Ti concentration along the shear planes (Fig. 1).

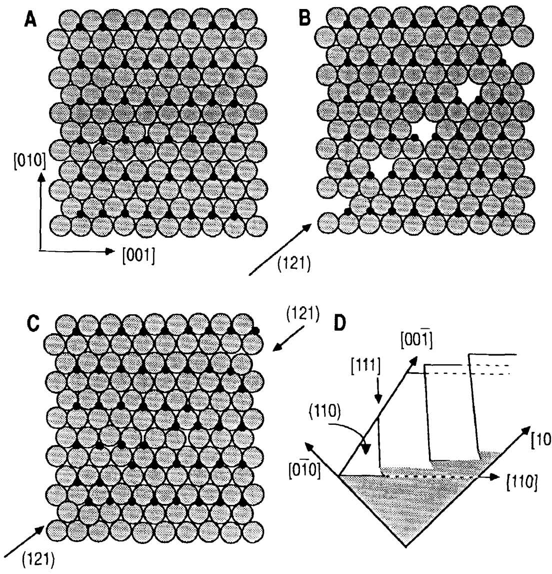

Fig. 1. Illustration of the CS plane formation process and the effect on the topography of the (110) surface. For simplicity, the structure is viewed parallel to the [100] direction in (A) to (C), while (D) is a perspective drawing that illustrates the effect of this operation on the (110) surface. (**A**) Idealized rutile structure; the larger circles represent O and the small black circles represent Ti. (**B**) Oxygen vacancies formed along the (121) plane. (**C**) Translation of one-half of the structure [the parts to the right of the (121) plane shown in (B)] by the vector ½[011] reestablishes the close-packed O framework and leaves the Ti atoms in antiphase positions. (**D**) The shear operations produce an ordered arrangement on steps on the (110) surface, as depicted in this perspective drawing. In this case, the steps are oriented in the [111] direction.

Several groups have produced STM images of single-crystal titania surfaces (*4*). None of these studies, however, produced atomic resolution images because four were carried out in air and the fifth in an electrolyte solution. Our $TiO_2(110)$ single crystal was cleaned, annealed, and characterized in UHV (*5*). Low-energy electron diffraction (LEED) patterns indicated the presence of a well-ordered, relatively defect-free surface (*6*). The crystal was then exposed to air for several days before it was introduced into the UHV STM chamber, heated at approximately 673 K for 2 min, and then "flashed" at approximately 973 K for 5 s. A (1×1) LEED pattern was found after this treatment that was identical to that observed after the initial preparation. Orientation of the crystal during STM analysis was determined from the LEED pattern. The orientations of the images are within $\pm 10°$ of the crystal orientation, the primary source of error being thermal drift.

We imaged the sample using a commercial STM head (WA Technologies, Cambridge, United Kingdom) controlled by "homemade" feedback electronics and software of conventional design. We "sharpened" the mechanically formed Pt tip in situ by applying a 90-V potential between the sample and the tip and passing 1 μA of current through it for several minutes. This procedure was repeated periodically to maintain tip resolution and stability. The dependence of the tunneling current on sample-tip separation was used to gauge the integrity of the vacuum gap. The standard vacuum tunneling equation was used to compute values of the effective barrier height between 4.2 and 5.0 eV (*7*). All of the images we present here were collected in the constant-current mode at a 2.0-V sample

---

G. S. Rohrer, Department of Metallurgical Engineering and Materials Science, Carnegie Mellon University, Pittsburgh, PA 15213.
V. E. Henrich, Surface Science Laboratory, Department of Applied Physics, Yale University, New Haven, CT 06520.
D. A. Bonnell, Department of Materials Science and Engineering, University of Pennsylvania, Philadelphia, PA 19104.

---

*To whom correspondence should be addressed.

bias with respect to the tip and a 0.1-nA tunneling current. The images are presented after the subtraction of a background plane, which eliminates the tilt of the sample that would otherwise overwhelm small variations and make atomic features undetectable.

Well-ordered areas were visible on most of the surface (> 50% when the tip was sharp), but were observed less frequently after several days of analysis. Two of the observed structures are discussed below. Auger electron spectroscopy performed immediately after the initial thermal treatment and at the end of the STM analysis showed that the level of C contamination had increased, presumably through exposure to background gases in the vacuum chamber. Fourier analysis and direct measurement of the images in Fig. 2, A and B, indicates that the rows oriented in the $[1\bar{1}1]$ direction have an 8.5 Å periodicity and a 1 Å corrugation height. The corrugation directed along the rows has a 3.4 Å periodicity and a 0.2 Å amplitude. The width of these rows seems to vary somewhat, and there are also numerous "missing cells." The bulk-terminated rutile lattice vectors have been added for comparison.

The image in Fig. 2B shows a larger area containing two ledges or atomic steps that are 2.2 Å in height, significantly less than the distance between adjacent (110) planes, which is 3.25 Å. Some regions of the image are either disordered or covered with adsorbates. A dark line cuts across the image in Fig. 2B in the $[\bar{1}13]$ direction (indicated by the solid arrow on the top left side of the image) and forms a step edge in the lower portion of the picture. This feature is oriented in the same direction as are the rows and ledges found in Fig. 3, which were acquired from a different area of the crystal surface. The largest rows in Fig. 3B, oriented in the $[\bar{1}13]$ direction, are approximately 20 Å wide and are parallel to the large steps visible in Fig. 3A. The height of the step in Fig. 3B is 9 Å. The detail in Fig. 3C shows that each row is composed of discrete units arranged in a roughly hexagonal pattern. The structure shown in Fig. 2 differs from the one shown in Fig. 3, and neither can be explained by a simple surface termination of the bulk unit cell or some combination of unit cells.

Two possible models can account for the observed surface structures; both rely on the presence of bulk nonstoichiometry. The geometries of both of the experimentally observed surface structures can be simply created by removing O from the surface layer in the appropriate pattern; we call this the ordered-surface oxygen vacancy (OSOV) model. However, an STM image is not simply a reproduction of the surface geometry but also depends on the surface density of states. Because all of the images were acquired at positive sample bias, electrons tunneled into unoccupied conduction band states that are predominantly Ti in origin. It follows that the light spots on the image reflect a greater density of Ti states, associated with the Ti atom positions, whereas the dark areas between the rows correspond to the absence of Ti states that is associated with the O atom positions. This result suggests that O must reside at the dark positions along the $[1\bar{1}1]$ and $[\bar{1}13]$ directions, whereas the other sites are vacant. However, at these positions, the tip is displaced downward by 1 Å, a rather large corrugation to arise from a change in the local density of states alone, especially considering that the presence of O atoms in these positions would presumably cause an additional opposite corrugation from purely geometric considerations. Because of this contradiction, the OSOV model does not seem plausible.

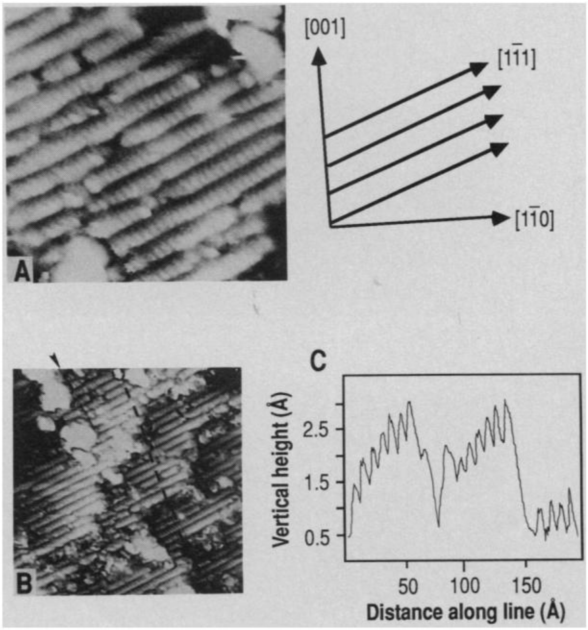

Fig. 2. (**A**) An STM image showing a 109 Å by 109 Å area of the $TiO_2(110)$ surface. The vertical resolution from black to white is 2 Å, with lighter shades corresponding to topographic peaks. (**B**) A 246 Å by 246 Å area that includes several steps. The vertical resolution from black to white is 2.8 Å. (**C**) Profile taken along the dotted line indicated by the open arrow in (B) shows the height of the steps.

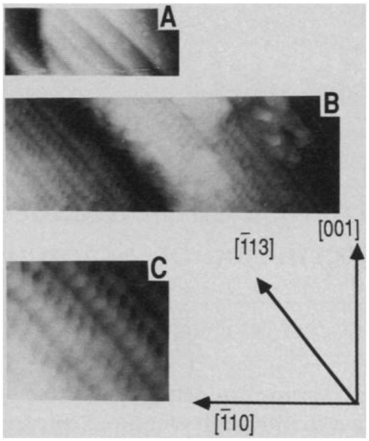

Fig. 3. (**A**) An STM image of a large terraced area (930 Å by 379 Å) with a series of steps oriented in the $[\bar{1}13]$ direction. The vertical resolution from black to white is 43 Å. (**B**) A more detailed scan (273 Å by 108 Å) of a region on the right side of (A). The vertical resolution from black to white is 9 Å. (**C**) An enlargement of a subsection of this image shows detail within each row.

The second model, the CS model, avoids this contradiction by assuming that the major row corrugations are actually steps that would result naturally from CS displacements. The CS displacements can occur along a variety of planes including the (121) family of planes. The (121) plane intersects the (110) surface along the $[1\bar{1}1]$ direction, the same direction in which the rows in Fig. 2 are oriented. The intersection of the $(1\bar{2}1)$ plane and the (110) surface is in the direction $[\bar{1}13]$, the same direction in which the rows in Fig. 3 are aligned. The CS displacement is always of the type $\frac{1}{2}[0\bar{1}1]$, which means that adjacent sections of the crystal are vertically displaced by 1.6 Å with respect to one another along the line normal to the (110) surface. Because the plane subtraction applied to each image removes any global slope, a stepped structure appears sawtoothed, so that the intersection of each CS plane with the surface appears as a depression or dark spot on the image.

The presence of excess Ti along the CS planes should result in a corrugation that is opposite to the geometric effect. However, corrugations due to alterations in the electronic density of states are usually some tenths of angstroms, so this effect should not be able to cancel the larger geometric effect. In fact, the observation that the corrugations in Fig. 2 are about 1 Å, which is less than the expected value of 1.6 Å, suggests that the presence of excess Ti in these positions compensates somewhat for the geometric effect. The disagreement between the expected and measured step height mentioned earlier may also be explained if each step is actually the sum of one (110) interplanar spacing and a CS plane. Although previous models of the reduced TiO$_2$(110) surface have not considered the possible existence of CS planes or their effect on the titania surface structure (*8*), the existence of these planar defects has been proposed by Firment and co-workers (*9*) to explain angle-resolved ultraviolet photoelectron spectroscopy (UPS) data from the reduced MoO$_3$(010) surface, another transition metal oxide surface that forms a variety of CS structures.

The spacing of the rows in Fig. 2 suggests that every sixth anion (121) plane is a CS plane and that the local composition in this area is Ti$_3$O$_5$, while the spacing of the rows in Fig. 3 suggests that CS occurs at every twelfth anion (1$\bar{2}$1) plane and that the local composition is Ti$_6$O$_{11}$. Although these phases are known to have a higher conductivity than rutile, they are still semiconducting, a fact verified by tunneling spectroscopy measurements. The 0.2 Å corrugations within the rows of Fig. 2 have a 3.4 Å spacing, which is very close to the spacing of Ti atoms (3.5 Å) along this same direction in the ideal rutile unit cell. Apparently, the nearest neighbor Ti atoms, separated by only 3 Å along the *c* axis, are not resolved. The distance between adjacent units within the rows of Fig. 3, measured parallel to the [110] direction, is approximately 6.4 Å, close to the bulk rutile unit cell spacing in that direction (6.5 Å). The distance between adjacent units in the [$\bar{1}$13] direction is 5.6 Å, which is the distance between the neighboring Ti atoms in that direction. However, each Ti atom is clearly not imaged, and a more detailed model for the atomic structure within the rows will have to be formed on the basis of additional experiments.

REFERENCES AND NOTES

1. M. D. Kirk *et al.*, *Science* **242**, 1673 (1988); N. J. Zheng, U. Knipping, I. S. T. Tsong, W. T. Petuskey, J. C. Barry, *J. Vac. Sci. Technol. A* **6**, 457 (1988); E. Garfunkel *et al.*, *Science* **246**, 99 (1989); X. L. Wu, Z. Zhang, Y. L. Wang, C. M. Lieber, *ibid.* **248**, 1211 (1990).
2. M. L. Norton, J. G. Mantovani, R. J. Warmack, *J. Vac. Sci. Technol. A* **7**, 2898 (1989).
3. L. A. Bursill and B. G. Hyde, *Prog. Solid State Chem.* **7**, 177 (1972).
4. S. E. Gilbert and J. E. Kennedy, *J. Electrochem. Soc.* **135**, 2385 (1988); K. Itaya and E. Tomita, *Chem. Lett.*, 285 (1985); K. Sakamaki, S. Matsunaga, K. Itoh, A. Fujishima, Y. Gohshi, *Surf. Sci.* **219**, L531 (1989); S. E. Gilbert and J. H. Kennedy, *Langmuir* **5**, 1412 (1989); *Surf. Sci.* **225**, L1 (1990).
5. The 1.0 mm by 5 mm by 1.6 mm titania sample was oriented to within ±0.5° of the (110) face by Laue diffraction and cut with a high-speed diamond saw from a single-crystal boule. The surface was polished by sequential reduction of the size of Al$_2$O$_3$ grinding media down to 1 μm. We reduced the crystal in UHV by annealing in a resistively heated Ta boat at a temperature above 900 K (on the basis of color) for 36 hours. After this treatment, the crystal was opaque and dark gray in color. The surface was then argon-ion–milled for 5 min at 2 kV and then subjected to 25 min of ion bombardment at 500 V using an estimated current density of 5 to 10 μA/cm^2. The crystal was then annealed at 823 K for 30 min in 1 × 10^{-7} torr of oxygen in order to reoxidize the surface and anneal out the damage produced by ion bombardment.
6. No UPS data were taken on this surface, although the LEED patterns were similar to those on the TiO$_2$(110) surfaces that exhibit no band gap defect surface states; see H. R. Sadeghi and V. E. Henrich, *Appl. Surf. Sci.* **19**, 330 (1984).
7. For details on the determination of the apparent barrier height, see J. K. Gimzewski and R. Moller, *Phys. Rev. B* **36**, 1284 (1987); N. D. Lang, *ibid.*, p. 8173; G. Rohrer and D. Bonnell, *J. Am. Ceram. Soc.*, in press.
8. W. Göpel, G. Rocker, R. Feierabend, *Phys. Rev. B* **28**, 3427 (1983); V. Henrich, *Rep. Prog. Phys.* **48**, 1481 (1985).
9. L. E. Firment, A. Ferretti, M. R. Cohen, R. P. Merrill, *Langmuir* **1**, 166 (1985).
10. Supported at the University of Pennsylvania by IBM Research and the NSF and at Yale University by NSF solid state chemistry division grant DMR-8711423. We thank Z. Zhang for assistance in preparing the sample surface.

12 July 1990; accepted 26 September 1990

Surface Displacements in the 1906 San Francisco and 1989 Loma Prieta Earthquakes

PAUL SEGALL AND MIKE LISOWSKI

The horizontal displacements accompanying the 1906 San Francisco earthquake and the 1989 Loma Prieta earthquake are computed from geodetic survey measurements. The 1906 earthquake displacement field is entirely consistent with right-lateral strike slip on the San Andreas fault. In contrast, the 1989 Loma Prieta earthquake exhibited subequal components of strike slip and reverse faulting. This result, together with other seismic and geologic data, may indicate that the two earthquakes occurred on two different fault planes.

IN ORDER TO UNDERSTAND FULLY THE tectonic setting of the 17 October 1989 M_s 7.1 Loma Prieta earthquake and the implications of this event for earthquake hazard assessment it is important to understand its relation to the most recent large earthquake on this part of the San Andreas fault system, the great 1906 San Francisco earthquake. In this report, we recalculate the horizontal surface displacements accompanying the 1906 earthquake as determined by historical triangulation measurements. We contrast the 1906 deformation in the Loma Prieta region with that occurring in the October 1989 earthquake and discuss the implications of these results for earthquake recurrence estimates and for future earthquake hazards in the Santa Cruz Mountains.

Much of what is known about the 1906 earthquake has come from analysis of geodetic survey measurements (*1*). The surveys consisted of horizontal angle measurements, made with a theodolite, taped baselines, and astronomic azimuth sightings. Pre-earthquake surveys were conducted in the San Francisco Bay region in the 1850s and 1880s; the region was resurveyed following the earthquake in 1906 and 1907 (1906–7).

In 1908 Hayford and Baldwin (*2*) published displacement vectors found by taking the difference of coordinates derived from the 1906–7 survey and coordinates derived from earlier measurements. Their results showed that displacements of several meters parallel to the San Andreas fault extended many kilometers from the fault trace. At the northern (Point Reyes) and southern (Monterey Bay) ends of the network, however, many of the displacement vectors derived by Hayford and Baldwin are opposite to the right-lateral motion observed across the San Andreas fault.

We suggest that the anomalous displacements reflect computational limitations rather than measurement errors. In the 1908 calculations it was assumed that Mount Diablo, Mocho, and Santa Ana, located 20 to 40 km east of the San Andreas fault (Fig. 1), did not move during the earthquake. Errors accumulate with distance from these arbitrarily fixed stations, and any true motion of these sites would bias the calculated displacements. Computational limitations prevented simultaneous inversion of all the data and also prevented determination of confidence intervals.

Given the considerable advances in computing in the last 80 years, we can adopt a different strategy. We reanalyzed the data using only repeated horizontal-angle and astronomic azimuth measurements, forego-

---

P. Segall, Geophysics Department, Stanford University, Stanford, CA 74305, and U.S. Geological Survey, Menlo Park, CA 94025.
M. Lisowski, U.S. Geological Survey, Menlo Park, CA 94025.